Article

Basin Scale Assessment of Landslides Geomorphological Setting by Advanced InSAR Analysis

Francesca Bozzano [1,2], **Paolo Mazzanti** [1,2], **Daniele Perissin** [3], **Alfredo Rocca** [2,*], **Pierfederico De Pari** [4] **and Marco E. Discenza** [4]

[1] Earth Sciences Department of Sapienza University of Rome, P.le Aldo Moro 5, 00185 Rome, Italy; francesca.bozzano@uniroma1.it (F.B.); paolo.mazzanti@nhazca.com (P.M.)
[2] NHAZCA S.r.l. Spin-Off of Sapienza University of Rome, via Cori snc, 00177 Rome, Italy
[3] Lyle School of Civil Engineering, Purdue University, 550 Stadium Mall Drive, West Lafayette, IN 47907, USA; perissin@purdue.edu
[4] Geoservizi S.r.l., Via Luigi e Nicola Marinelli n.2, 86025 Ripalimosani (CB), Italy; depari@geoservizisrl.net (P.D.P.); discenza@geoservizisrl.net (M.E.D.)
* Correspondence: alfredo.rocca@nhazca.com; Tel.: +39-06-9521-6501

Abstract: An extensive investigation of more than 90 landslides affecting a small river basin in Central Italy was performed by combining field surveys and remote sensing techniques. We thus defined the geomorphological setting of slope instability processes. Basic information, such as landslides mapping and landslides type definition, have been acquired thanks to geomorphological field investigations and multi-temporal aerial photos interpretation, while satellite SAR archive data (acquired by ERS and Envisat from 1992 to 2010) have been analyzed by means of A-DInSAR (Advanced Differential Interferometric Synthetic Aperture Radar) techniques to evaluate landslides past displacements patterns. Multi-temporal assessment of landslides state of activity has been performed basing on geomorphological evidence criteria and past ground displacement measurements obtained by A-DInSAR. This step has been performed by means of an activity matrix derived from information achieved thanks to double orbital geometry. Thanks to this approach we also achieved more detailed knowledge about the landslides kinematics in time and space.

Keywords: landslide; state of activity; synthetic aperture radar interferometry; Persistent Scatterers; ERS; Envisat

1. Introduction

In the last 40 years, several techniques for mapping and assessing slope movements have been developed, thus allowing for most reliable and fast investigation [1–4]. Geomorphological landslide mapping is a complex problem as it is affected by several factors, such as the availability of the diagnostic data, the scale of the analyses and the final objective of the performed investigation [2,5–8]. A suitable cartographic representation of landslide bodies is the first step in addressing such a hazard for a given area. Depending on the final purpose, several types of landslide mapping can be performed, such as landslide inventory, landslide typology and landslide state of activity maps. The standard approach in landslide mapping procedure is mainly based on the expertise of the surveyor, therefore is affected by uncertainties and sometime subjective information.

If a landslide inventory map represents a snapshot of the territory at a given moment [8], the state of activity map requires assumptions also about the temporal evolution of the given processes.

Therefore, quantitative information about displacements that have occurred represents a valuable source of information for landslide state of activity assessments.

Recently, the contribution of remote sensing techniques to natural hazards risk reduction has dramatically increased. Satellite InSAR, in particular, has proven to be a reliable methodology for landslide investigation [9–14].

Specifically, Satellite Advanced Differential Synthetic Aperture Radar Interferometry (A-DInSAR), namely Persistent Scatterers Interferometry (PSI), Small Baseline Subset (SBAS) and similar techniques [15–18], has greatly increased the range of landslide research and monitoring applications since their development in the early 2000s. Because of the increased practical fruition of the results provided by such techniques, A-DInSAR is becoming a reality today not only for scientific studies but also by professional applications [12,19]. One of the key features of A-DInSAR is the ability to provide quantitative results about past ground displacements. At present, such results are not achievable with comparable accuracy using any other technique.

However, as noted by other authors [12], InSAR data need to be integrated with other investigation techniques and prior information to take advantage of this tool. Field surveys and interpretation of aerial photos and other remote sensing data (both ground based and satellite based) are useful not only to properly interpret InSAR results but also to attain basic information about the investigated area to design suitable InSAR analyses [20–23].

In this paper, we integrate the above-mentioned traditional and recent (in situ and remote sensing based) techniques in order to infer quantitative data to be applied to the landslide risk mitigation strategies in an area intensively affected by such a type of risk. The study area is located in central Italy, in the eastern sector of the Apennine chain. It is illustrative of similar worldwide geological and geomorphological contexts, and its specific setting is described in the next section.

2. The Study Area

The investigated basin (approximately 20 km^2) is located in the Abruzzi region (Italy), near the villages of Casacanditella, Filetto and San Martino sulla Marrucina (Figure 1). The area is situated in the Periadriatic zone facing the Maiella relief (approximately 20 km from the Adriatic coast). It is a typically hilly area with N-S-trending valley floors, incised by the Dendalo and Vesola San Martino streams, with absolute heights ranging between approximately 460 m above sea level (a.s.l.) on the surrounding hills and 150 m a.s.l. on the stream floor, thus generating, on average, moderate slope energy.

Figure 1. Location of the study area. The red box identifies the study area. (**a**) A 3D image shows the watershed (blue line) bounding the basin under investigation. The images are extracted from Google Earth®.

2.1. Geological–Structural Characteristics

From a structural standpoint, the investigated area lies along the outer margin of the Apennine chain [24], slightly west of the Ortona-Roccamonfina line [25]. This roughly NNE–SSW-trending alignment is the zone of junction between the two large arcs forming the Apennine thrust-and-fold belt system [25–27]. The chain thus consists of wide E-dipping thrust sheets and thrusting calcareous lithotypes over arenaceous-clayey deposits [28,29].

In the investigated area, the bedrock is composed of a thick marine succession of the upper Pliocene-Pleistocene *pro-parte* (p.p.), known in the literature as the Mutignano Formation [24,30]. In its lower part, the succession presents grey-blue marly clays, often interbedded with sands that become increasingly frequent and thick moving upwards. In its upper part, it contains grey and ochre silty sands, with pelitic levels and occasional arenaceous and conglomeratic intercalations.

Fluvial and lagoonal deposits of Pleistocene p.p.-.upper Pleistocene p.p. age occur along the top portions of reliefs and near morphological terraces [31–33]. These deposits embed polygenic conglomerates in a sandy-silty groundmass, with local sandy layers and clayey and peaty intercalations.

Extensive Holocene fluvial and detrital-colluvial deposits are observed along fluvial incisions and slopes [31,32]. These terrains consist of clayey-silty and sandy-silty deposits, frequently evolving into gravels and pebbles or cobbles.

Structurally, the investigated area has numerous high-angle normal and strike-slip faults [24,28,30], clearly dislocating the bedrock lithotypes. These faults, covering a small surface area, have throws of meters to tens of meters. The primary fault systems have approximately N–S, E–W, SW–NE, SE–NW and SSE–NNW directions [24,34], although non-systematic faults with different orientations are also found. The above described tectonic features progressively downthrow the Mutignano Formation towards the main valley floors. Finally, the formation has a generally monoclinal and gently NE-dipping pattern, and its strata have an inclination of 5° to 15° (Figure 2).

2.2. Geomorphological Characteristics

The geomorphology of the Periadriatic sector of Abruzzi is strongly controlled by its local geological–structural setting and by the recent evolution of the Apennine chain [31,35]. The above-mentioned tectonic features control the configuration of the leading drainage lines and morphological ridges of the investigated area [33,36]. In particular, the shaping of the reliefs and the geomorphological evolution of this sector of the region are largely dependent on slope movements [35,37,38].

The investigated area is affected by several landslides and slope deformations [38], most of them reaching the Dendalo stream valley floor. These processes originate from various geological and geomorphological factors (i.e., tectonic features, soil characteristics, surface water dynamics, land uses, and seismicity). In this scenario, slope instabilities generally arise along tectonic lines and in areas affected by strong surface erosion [37,39]. The distribution and features of these landslides are directly related to the geology of the area and to its high-angle tectonic lines [39]. Indeed, structural lineaments represent elements of weakness along which the landslide can move preferentially. Conversely, the pattern of the rupture surface in the intermediate-low sectors of the landslide bodies depends on the setting layout of the bedrock. Furthermore, landslide typologies are of course influenced by outcropping terms. Because of the presence of different types of soils, primarily characterized by the presence of silty sands and pelitic terms generally belonging to the Mutignano Formation, the typical instability processes detected in the study area can be classified as slides, earth-flows and complex landslides.
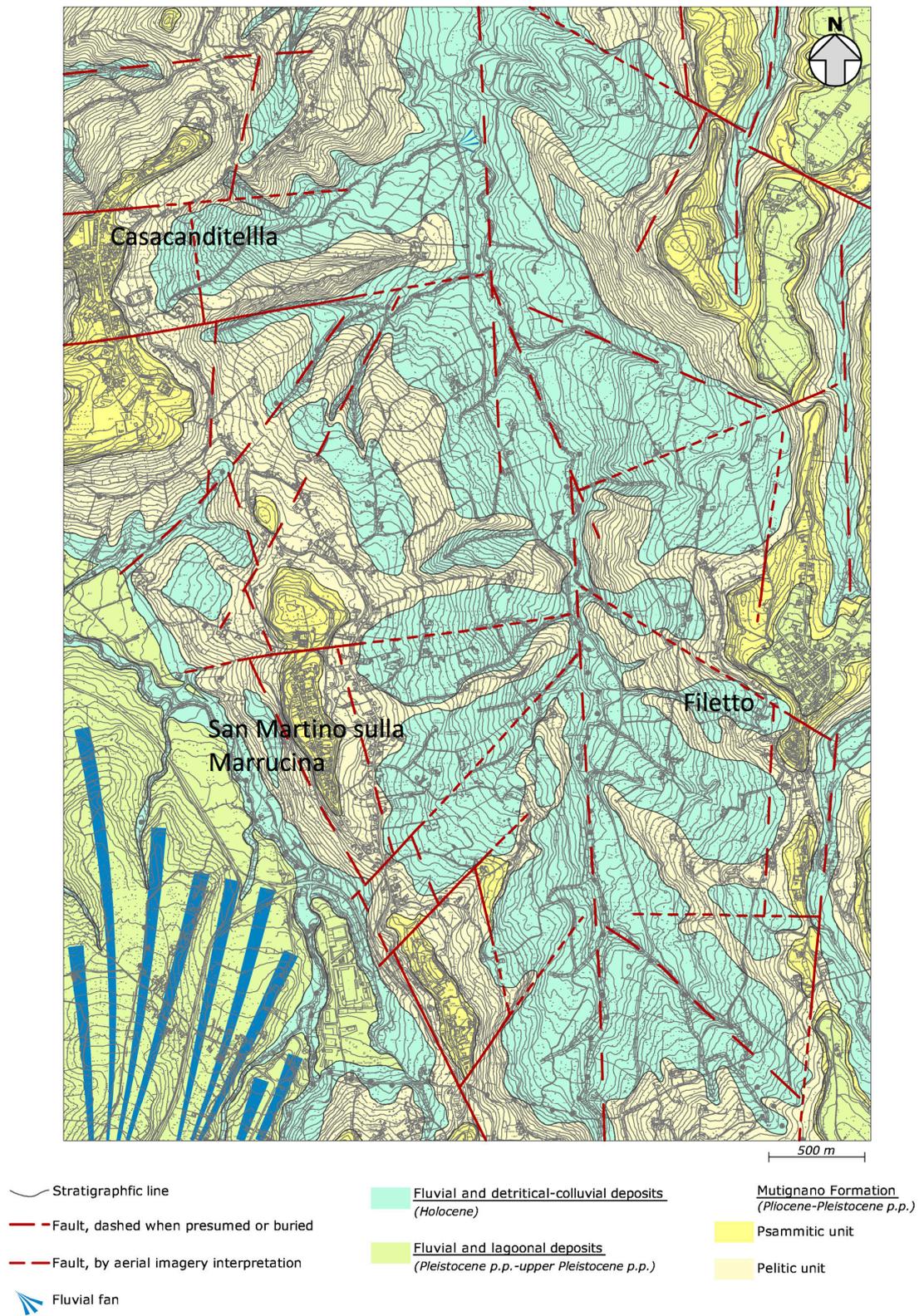
Figure 2. Geological map of the study area produced by the authors.

3. Landslides Mapping

3.1. Methods

A detailed mapping of landslides was performed using geomorphological field surveys and the interpretation of multi-temporal aerial photos. The primary objective was to properly define a landslide inventory for the study area, characterizing each detected phenomenon in terms of landslide typology and providing a preliminary indication about the state of activity [40].

The landslides mapping of the whole study area has been carried out starting from the analysis of data available in literature. In particular, during the early stages of the study, regional and national maps of landslides, available for the whole Italian country (i.e., Piano di Assetto Idrogeologico - PAI - database and Inventario dei Fenomeni Franosi in Italia - IFFI - database) [41,42], have been acquired. Starting from such information, a detailed local-scale mapping has been obtained by specific field surveys performed between October 2010 and June 2013, on the whole study area. These surveys have been carried out to define for all landslide phenomena the main morphological elements and information about the landslide areas and the related state of activity.

At this regards, an important contribution has been provided by the analysis of multi-temporal datasets of aerial photos, useful to define the spatial and temporal evolution of the slopes. Specifically, the following four datasets were used: 1954 (Average Scale (A.S.) 1:33,000), 1987 (A.S. 1:33,000), 2002 (A.S. 1:13,000), and 2007 (A.S. 1:5000). Analyses of stereoscopic pairs of images allowed for the mapping of the main landslide bodies as well as for the identification of geomorphological and hydrographical features that are also related to the temporal morpho-evolution of the active processes in the area.

3.2. Results

The analysis of aerial photos from 1954 to 2002 combined with field surveys allowed us to identify and map 97 landslides within the study area. Landslides affect most of this portion of the Dendalo stream basin and were classified as slides (15 processes), earth-flows (41 processes) and complex mass movements (41 processes) [43] (Figure 3a).

In general, the multi-temporal aerial photos analyses showed the presence of current slope instability phenomena since 1954, indicating that the detected landslides are pre-existing and, in many cases, quite old. These phenomena could be placed into the context of the complex geological, structural and geomorphological conditions of the area, and they are not directly connected with human activities in the area in recent decades.

The landslide deposits are related to the mobilization of the pelitic and psammitic lithologies of the Mutignano Formation, especially on the middle and lower portions of the slopes. In the mainly pelitic areas, the geomorphological elements related to the largest landslide phenomena, such as niches, scarps and counterslopes, are highly altered and degraded and often modified by the strong anthropic activity in the area. Landslide areas range from a few hundred square meters to several square kilometers. Complex landslides are the widest and deepest phenomena, with failure surfaces often in the range of several tens of meters. Conversely, the earthflows are smaller and less deep (mean thickness of several meters).

Displacement mechanisms are well identified using landslide crowns patterns (usually evident even if partially affected by deterioration), the presence of clear counterslopes and landslide terraces. The detected phenomena are primarily characterised as complex, wide landslide systems, in which it is not always possible to identify and bound individual instability phenomena. Finally, local processes related to viscous deformation of shallow material (creep and/or solifluction) affect the steeper slopes or portions of slopes surrounding the landslide areas. Most of the landslides show moderate signs of reactivation, thus demonstrating limited evolution rates.

Based on these investigation methods, the state of activity appears to be generally dormant, with a return time of a few years to some tens of years. The stabilized phenomena are represented by very extensive landslide movements along the Dendalo stream valley floor. Using field surveys

and multi-temporal aerial photos, we could detect some active or suspended phenomena, represented by some fairly shallow landslides and by the system of slides and complex slides occurring SE of the village of San Martino sulla Marrucina (Figure 3b). Their stage of activity is generally advanced or senile, exhausted only for the inactive and more ancient phenomena. According to [43], we can describe the distribution of activity of the landslides as mostly "retrogressive" and rarely it may be characterized by a complex combined movement, "advancing" and "retrogressive" at the same time.
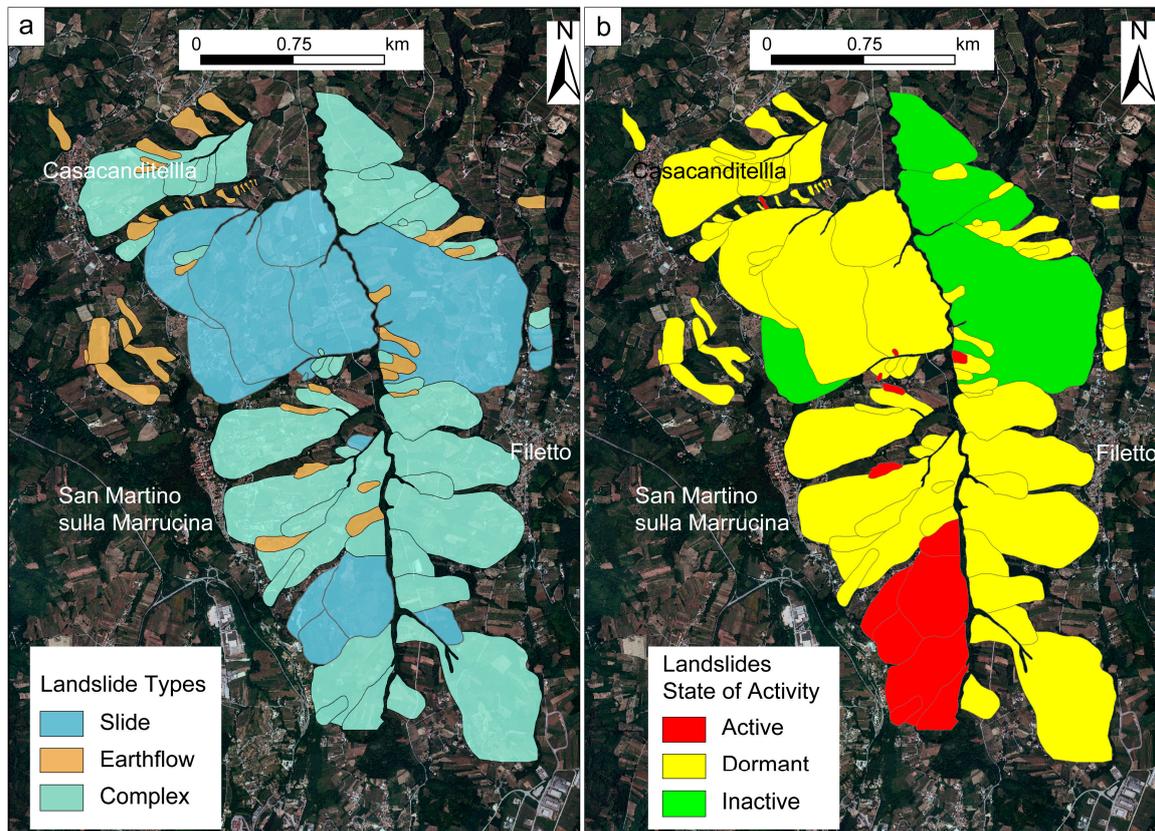

Figure 3. (**a**) Landslides mapped in the study area, classified in accordance to [43]; and (**b**) landslide state of activity inferred by geomorphological elements observed by aerial photos interpretation and field surveys. Images in background are extracted from Google Earth®.

4. A-DInSAR Analyses

Information about the temporal and spatial evolution of landslide processes (landslide mapping, spatial evolution, state of activity) attained using multi-temporal aerial photos represents the first stage of a large-scale slope instability investigation [44–48].

However, this widely used methodology has several limitations: (i) it is strongly discontinuous in time (the availability of data depends on the presence of archived aerial photos acquired in the same area over time); (ii) as in our case study, datasets are often heterogeneous in terms of spatial scales as well as film type (the availability of black and white and color photos); (iii) the definition of the states of activity of several processes are directly related to the presence of geomorphic elements (this aspect is crucial if anthropic activities such as agriculture occur in given area); (iv) the identification of diagnostic elements is strongly affected by operator subjectivity; and (v) the results are only partially quantitative and not highly accurate [4].

To define in detail the deformational behaviors of slopes and improve the knowledge of the spatial and temporal evolution of landslide in the study area, we performed A-DInSAR analyses.

4.1. Basic Principles and Applications

Over the last two decades, classical DInSAR analyses, performed by coupling SAR images to generate differential interferograms have been largely adopted as a tool to investigate ground deformation processes.

DInSAR has proven to be a very useful methodology to analyze several ground deformation phenomena, such as coseismic and post seismic deformations [49,50], volcanic deformation processes [51,52], and ice and glacier dynamics [53,54]. Landslide processes have also been studied using the DInSAR technique [14,55–58]. However, several limitations affect DInSAR: artifacts due to the atmosphere phase screen (APS), the presence of residual topographic contributions, and decorrelation effects (both temporal and geometrical), which can prevent the observation of displacement information or reduce the accuracy of the results.

Advanced DInSAR (A-DInSAR) techniques are an effective solution to reduce some of the limitations of standard DInSAR analysis [10,15,16,59–64]. All A-DInSAR approaches are basically characterized by the exploitation of large, multi-temporal data-stacks to generate several interferograms, thus achieving higher redundancy of interferometric results. One of the most known approaches is the so-called Persistent Scatterers Interferometry (PSI), which is based on the information achieved by pixels of the SAR images characterized by high coherence over long time intervals [10,15,60]. Generally, constructed structures, such as buildings, bridges, dams, railways, or pylons, or natural elements, such as outcropping rocks or homogeneous terrain areas, can represent good Persistent Scatterers (PS).

Unlike the SBAS approach [16], standard PSI is based on the generation of interferograms using a common master SAR image. Point-like scattering pixels remain coherent for the entire observation period, and they do not suffer from temporal and geometrical decorrelation effects, thus also allowing the generation of interferograms using image pairs characterized by long temporal and normal baselines. Using this principle, almost all images that constitute a given stack can be used to perform multi-temporal A-DInSAR analyses. The latter point is crucial for the investigation of past displacements because, in this case, information can be attained only from archived SAR data, and it is fundamental to not waste the possible contributions of any SAR acquisition. Every image contributing to an A-DInSAR analysis represents "one sample" in a given time series of displacement. For some deformation phenomena, such as landslides, it is very important to attain a time series as detailed as possible.

However, it is worth noting that A-DInSAR techniques are also affected by some limitations. First, because only objects which are good "radar reflectors" can be analyzed, they have an inability to attain information over highly vegetated areas. This aspect is not secondary as landslides often involve non-urban areas, and, if any corner reflector had been installed, there is no way to overcome this issue for past-oriented A-DInSAR analyses. Moreover, because of the cyclic nature of the phase signal, it is not possible to observe very rapid displacements [65]. Furthermore, satellite SAR interferometry is affected by the capability of observing displacements only along the so-called Line of Sight (LOS), which is the sensor-target direction [66].

4.2. A-DInSAR Data Processing

For the present case study, we performed A-DInSAR analyses of past displacements using four SAR data-stacks from the ESA archive ranging in the time span 1992 to 2010. Specifically, ERS1/2 data were selected for the 1992–2001 period, and Envisat data were selected for the 2002–2010 period. Large-scale analyses have been performed on a portion of the SAR images frame large approximately 11×11 km^2, thus covering an area larger than the Dendalo basin. For both periods, we analyzed both ascending and descending datasets. In this case, because of the N–S oriented basin, we had to contend with the east and west aspects of the slopes; thus, to properly observe the possible displacements on all slopes, we had to select datasets acquired in ascending and descending orbital geometries (Table 1). Moreover, a Digital Elevation Model having 30 m resolution was used to compute the differential

interferograms (i.e., to subtract the topographic phase component from the interferometric phase) and to geocode the PS results.

Table 1. Archived data stacks selected for the A-DInSAR analyses.

Satellite Data-Stack	ERS Descending	ERS Ascending	Envisat Descending	Envisat Ascending
Images (num.)	71	47	47	54
Period covered	June 1992–January 2001	June 1995–December 2000	November 2002–September 2009	February 2003–September 2010
Master image	26 June 1997	16 June 1998	18 August 2005	18 October 2006

We performed the interferometric analyses using Sarproz software [64], which is specifically developed for multi-image InSAR analyses, such as PS [10] and QuasiPS (QPS) [17].

For each dataset, all images have been related to a single master image; more specifically, the selected masters are reported in Table 1. The master image was selected by considering the normal and temporal baselines, thus trying to reduce the decorrelation effects. After all images were co-registered to the master image, the reflectivity map (i.e., the multi-temporal amplitude value for each pixel) and the amplitude stability index (ASI, i.e., the coefficient of variation of the amplitude) were generated and used as quality estimator for the selection of PS candidates (PSC) in the PSI procedure.

The Methodology Adopted

The multi-image interferometric analysis has been performed with a combined technique, based on PS [10] and QPS [17] integration. In particular, this hybrid approach is performed by taking advantage of two different image connection graphs used for the different methodologies.

1. In a first step, as is standard for the PS method, the so-called "star" graph has been used (Figure 4a), thus connecting all slave images to a single master image to generate interferograms.
2. Moreover, by using the QPS method [17], we also connected the same images using the Minimum Spanning Tree (MST), which is a weighted graph to connect images to maximize spatial coherence (Figure 4b).

The connection based on the star graph ensures a temporal continuity and improves the capability of unwrapping the phase signal to generate reliable displacement time series, while interferograms obtained from the images connected in this way may provide wider information if compared with those computed starting from the star graph because of the higher number of coherent scatterers.

The interferometric phase signal, $\Delta\phi_{int}$, is the result of multiple contributions. For the sake of simplicity, we here indicate only the following terms:

$$\Delta\phi_{int} = \Delta\phi_{topo} + \Delta\phi_{displ} + \Delta\phi_{atmo} + \Delta\phi_{noise} \tag{1}$$

where $\Delta\phi_{topo}$ is the contribution of the residual topographic height (H) after DEM subtraction from interferograms, $\Delta\phi_{displ}$ is the searched displacement (D) information, $\Delta\phi_{atmo}$ is the disturbance caused by the Atmospheric Phase Screen (APS), and $\Delta\phi_{noise}$ is the non-removable phase disturbance. To properly estimate the displacement (D) and the topographic height (H) values, we selected a set of PS candidates (PSC) using an ASI threshold to choose very stable pixels in terms of the amplitude signal over the analyzed period.

All PSCs were then connected to create a redundant spatial network, and H and D were estimated along the connections starting from a linear model to infer unknown displacement. Once we found H and D values for every connection, those values were integrated over the PSCs to estimate the APSs (one for every image of the dataset) starting from the residual phase components. Once the APSs have been attained, a second estimation is performed on a much larger set of points, which will represent the final step of the PSs after a final temporal coherence threshold to select the final results.
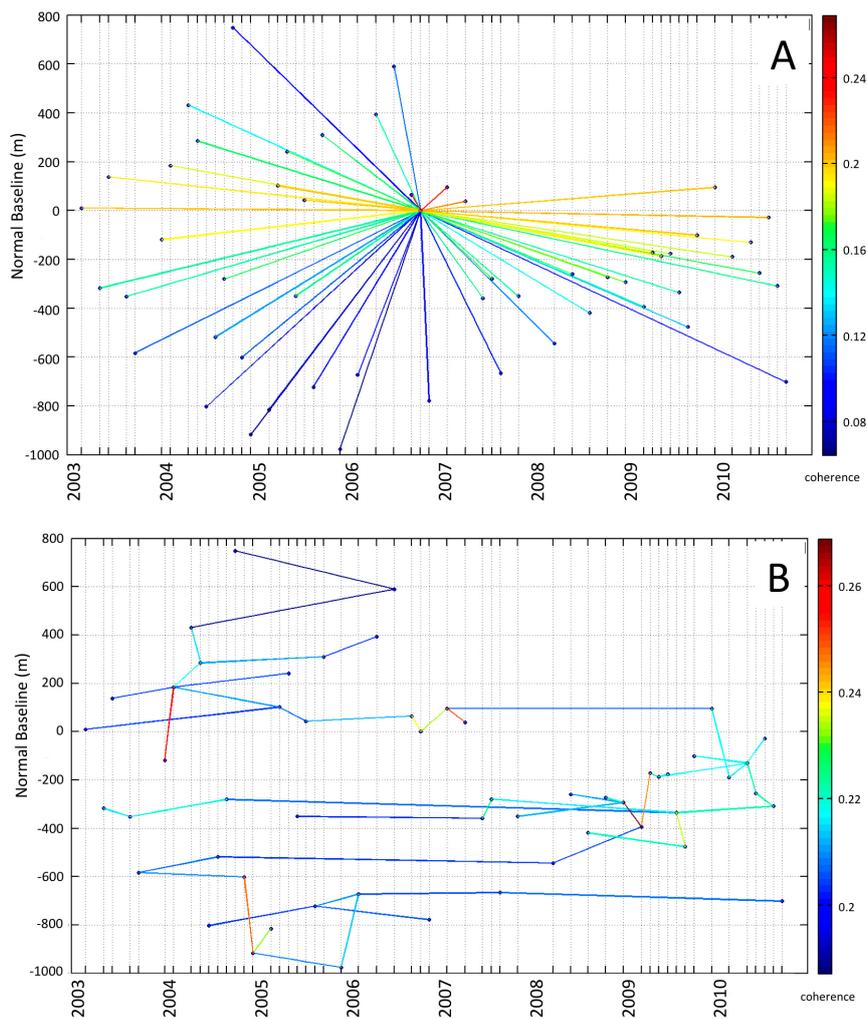
Figure 4. Graphs used to connect images relating to temporal baseline (*X* axis) and normal baseline (*Y* axis). Every dot represents an image, while every line represents an interferogram. Colors from blue to red show increasing value of spatial coherence. It is worth noticing different values of spatial coherence achievable from: "star" graph (**A**); and Minimum Spanning Tree (MST) graph (**B**). In particular, minimum values are considerable higher for MST graph. The example refers to the Envisat descending dataset.

4.3. A-DInSAR Results

In Figure 5, the A-DInSAR results are related to the ERS and Envisat periods. PSs are shown as colored dots. Colors are related to displacement rates (mm/year) along the LOS.

Dots from yellow to red show displacements away from the satellite, and dots from light blue to dark blue indicate displacements towards the satellite. Green dots represent points not affected by displacement in the investigated period. A-DInSAR results have been computed with respect to a reference point (white star in Figure 5) assumed as stable and located outside of the study area. Red polygons indicate landslide bodies mapped through the interpretation of aerial photos and field surveys.

The A-DInSAR results cover 27 landslides of the total of 97 affecting the study area (less than 30% of the number of phenomena). However, it is worth noticing that these 27 landslides are the largest ones on the overall study area, thus a large portion of the basin affected by instability processes has been investigated thanks to the presence of sufficient PSs within the landslide bodies. The landslides without PS are mainly represented by small and very small earthflows located in secondary valleys, where no buildings or other structures as potential good radar targets are present.

For the sake of completeness, we want to focus on some peculiar features related to the spatial distribution of the A-DInSAR results.

First, the main urbanized areas are settled on the quite flat hilltops, offering many good scatterers as potential PSs. Starting from interpretation of aerial photos and field surveys, we derived that almost all landslide processes seemed not to affect such villages. This information, indeed, is also confirmed by the A-DInSAR results, which substantially show stable PSs over the urbanized areas (see ellipses A, B and C in Figure 5). Moving down from hilltops, the slopes degrade gently to the streams. Especially on the western slopes, many PSs showing displacement information are present in both the ascending and descending geometries.
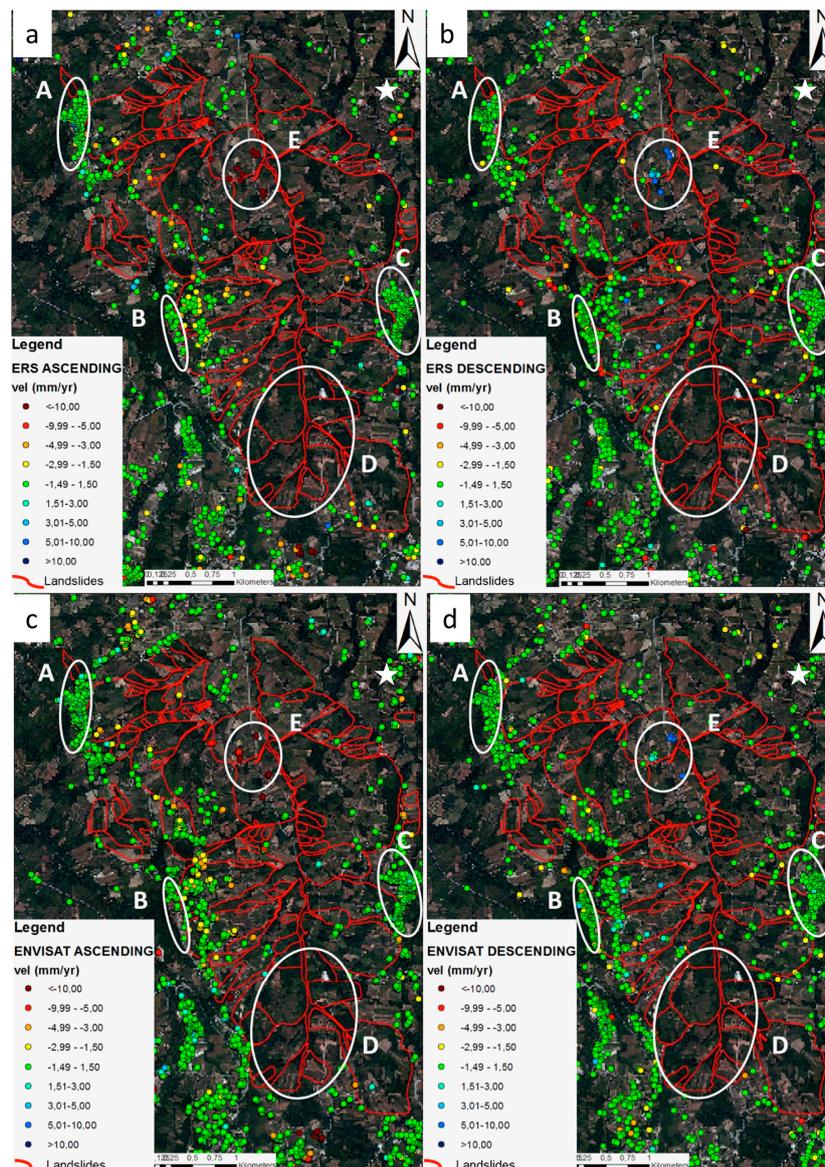

Figure 5. A-DInSAR results: (**a**) ERS ascending; (**b**) ERS descending; (**c**) Envisat asc; and (**d**) Envisat desc. PSs are presented as colored dots. Colors from yellow to red state displacements away from the satellite, while dots from light blue to dark blue state displacements toward the satellite. Values are expressed in millimeter/year. The white star indicates the location of the reference point. Red polygons indicate landslide bodies mapped thanks to aerial photos interpretation and field surveys. A, B and C ellipses indicate urbanized areas. D ellipse indicates an area where no PSs have been detected because of absence of good scatterers. E area indicates the area affected by strong horizontal displacements discussed in Section 4.4.

State of Activity

Thanks to the availability of the multi-temporal archive data (in the present work, both aerial photos and satellite SAR images), the evolution of the state of activity of the detected landslides has been assessed. As stated above (Section 3.2), starting from the analyses of the airborne optical images and field surveys, a given state of activity has been assumed for each landslide (Figure 3) based on geomorphological criteria. Several field surveys have been performed in different years to evaluate the state of activity, and very similar results were attained in 2010, 2011 and 2012, suggesting a very slow displacement pattern for landslides characterized as "dormant". Furthermore, using the ERS and Envisat A-DInSAR results, which provided quantitative data (i.e., the detection of targets affected by displacements), the landslide state of activity for the two analyzed periods has been assessed.

In this study, we present an approach based on the observation of double orbital geometries to assess the period of activity for both the ERS (1992–2001) and Envisat (2003–2010) datasets by considering the deformation rates observed by A-DInSAR. Several deformation rate thresholds to define whether a landslide process is reactivated have been chosen by many authors [4,67–71]. As a general rule for this case study, only PSs characterized by velocities greater than 2 mm/year have been selected as active period markers. In Figure 6 the basic operating principle of the proposed method is explained. A quite similar approach has been used by Cigna et al. [4] to assess the reactivation and state of activity of landslides comparing different PSI datasets. The primary difference here is that the input data are not differentiated in time (e.g., ERS and Envisat), but they are contemporary (e.g., both ERS and Envisat) and belonging to different orbital acquisition geometries (i.e., ascending and descending).

		ORBITAL GEOMETRY 2		
		Unstable PS	Stable PS	Not enough PS
ORBITAL GEOMETRY 1	Unstable PS	Period of activity	Period of activity	Period of activity
	Stable PS	Period of activity	Period of inactivity	Undefined activity
	Not enough PS	Period of activity	Undefined activity	Undefined activity

Figure 6. State of activity matrix based on combination of double orbital observation geometries (ascending and descending).

Because landslides in the herein studied basin are located on both west and east facing slopes, even if PS data are available for both dataset results, displacements are sometimes visible in only one of them because of the direction of the LOS. Therefore, the consideration of both geometries allows the detection of displacements that might go unseen using only one geometric condition. The state of activity matrix is quite preventive, and thus the detection of unstable PSs, even in only one geometry, is enough to assess the related landslide as "active" in that period. With the same logic, the detection of stable PSs in only one geometry is not sufficient to consider the landslide as "inactive" in the considered period. Moreover, the inactivity is considered only when the presence of stable PSs is confirmed by both geometries. In Figure 7, the results from the activity matrix application are shown. For both the ERS and Envisat periods, green polygons define landslides characterized by the presence of stable PSs, whereas red polygons identify the presence of unstable PSs. Empty polygons identify landslides with missing or insufficient PSs.

After the comparison of Figure 7c,f, we can assert that the state of activities of the landslides remains roughly similar in both the analyzed time intervals (1992–2001 for ERS and 2001–2010 for

Envisat). It is worth noting that two little earthflows and some little complex east-facing landslides in the central part of the study area are present in the Envisat time interval.

The A-DInSAR results were also useful in defining spatial evolution in time of observed processes. In Figure 8 an example, representative of the interpretation that has been performed for several individual landslides is shown: a large slide, belonging to a more generalized slope deformation phenomenon experienced a gradual retrogression, detected by PSs showing displacements from 1992 (the beginning of the period covered by the ERS data) to 2003 (the beginning of the Envisat observation period). This outcome (observed on results from different datasets) is a confirmation of the role played by A-DInSAR in the slope dynamics investigation. The detection and quantitative measurement of past displacements represent an opportunity to overcome the limitations of standard investigation methods, which are usually based on the identification of geomorphological effects, not always easily observable.
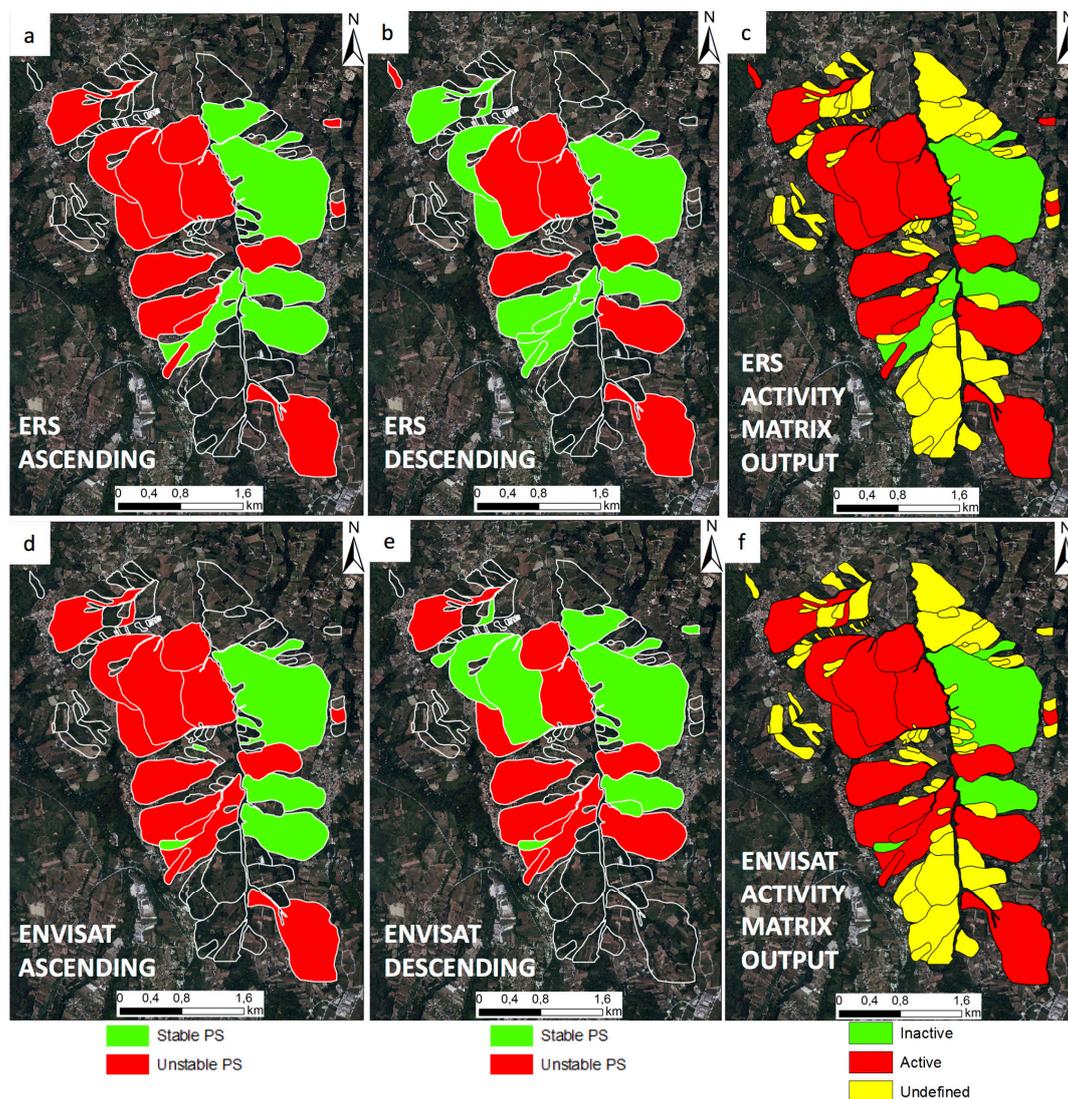

Figure 7. Results from the activity matrix: (a, b, c) ERS (1992-2001) data and (d, e, f) Envisat (2003-2010) data. Green polygons identify presence of stable PSs within the mapped landslide; red polygons identify presence of unstable PSs; empty polygons show missing or insufficient PSs. The state of activity results (shown in c, and f) are derived from both orbital geometries combination. Color codes are the same used for the state of activity matrix in Figure 6.
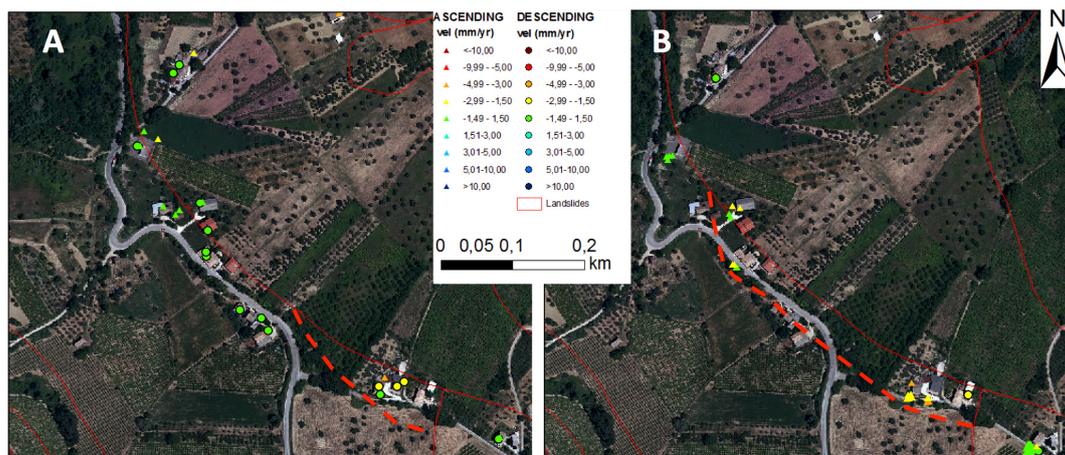
Figure 8. Example of crown retrogression for a large slide in the northwestern part of the study area: (**A**) ERS (ascending and descending) results (1992–2001); and (**B**) Envisat (ascending and descending) results (2003–2010). The example shows progressive evolution of the expansion phenomenon over time. The red dashed line represents the gradual retrogression.

4.4. Landslides Type of Movement

The combination of results achieved by ascending and descending datasets also allowed to better define the type of movement of the investigated landslides. At this regards, it is interesting to observe an example where an area is characterized by PSs of different orbital geometries which show different values or direction of displacement. More in detail, a small area very near to the Dendalo stream (ellipse E in Figure 5), is interested by results from the ascending dataset showing movements away from the satellite (generally evaluated as a "subsidence-like process"), whereas the descending results show movements towards the satellite (generally considered as an "uplift-like process"). Moreover, such behavior is observed in both the ERS and Envisat datasets, thus in different periods.

The combination of the double-geometric datasets allowed the derivation of the vertical and horizontal (E-W) components of the movement [72]. The area, in fact, is on a very gentle slope (from 2° to 7°) that marks the foot of a large landslide composed of several coalescent bodies. By considering the slope aspect, oriented nearly east, it was possible to use these results to interpret real local displacements in terms of both orientation and magnitude (Figure 9).

The results clearly highlight the overall slope deformation behavior, primarily characterized by horizontal displacements, especially near to the landslide foot, as typical for this type of earth slide. Moreover, the portion of the landslide affected by slightly stronger vertical components is located very near to the crown of the lowest landslide body, during both the ERS and Envisat periods. In addition, this effect is congruent with the types of movement (especially in terms of orientation of displacements) affecting this landslide portion.

It is worth noticing that, as is clear in the example above, the information related to the different orientation of displacement vectors along the slope (Figure 9) help to infer the characteristics of the sliding surface. Furthermore, differences in space of such displacements can be directly related to the presence of secondary sliding surfaces. In this way, A-DInSAR revealed to be a useful tool to confirm or adjust the landslides mapping obtained by traditional techniques.
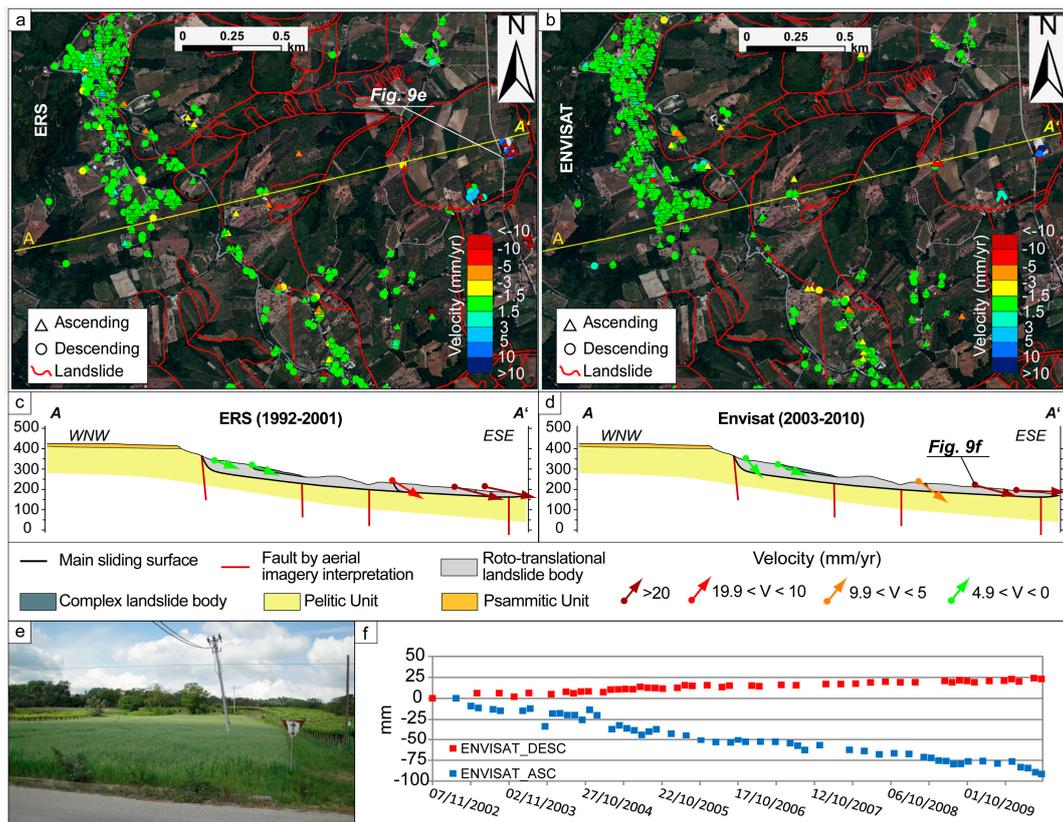
Figure 9. Section of an investigated landslide characterized by strong horizontal component: (**a**, **b**) Ascending and descending PS results related to ERS and Envisat datasets, respectively. The yellow line A-A' identifies the landslide section track drawn beside for: ERS (**c**); and Envisat (**d**) datasets. Colored vectors represent displacements along the slope taking into account vertical and horizontal components derived by combining ascending and descending results. (**e**) Pylon affected by instability near the landslide foot. (**f**) Ascending and descending time series of displacement related to PSs used to derive the indicated displacement vector for the Envisat period.

5. Discussion

A-DInSAR has revealed to be an excellent support to the understanding of the landslides processes in the Dendalo basin. Most of these processes have proven to be suitable for being studied by selected techniques also because their typical velocity of deformation is not too high to be observed by satellite A-DInSAR. However, using these results, we can deduce some other general considerations less related to the present case study. A general look at the results of the entire study area (Figure 5) reveals more detailed A-DInSAR information attained for the east-facing slopes than for the opposite slopes. As stated by several authors [4,20,21,66,73,74], several factors can affect the quality of A-DInSAR results for a given area. These factors are related to the SAR system features and the geomorphological local conditions [21]. In the context of ground deformation phenomena, this point is crucial for landslides characterized by various directions of movement (vertical and horizontal) and variable slope orientation. The use of double geometric investigation (ascending and descending orbits) was fundamental for facing with both west- and east-facing slopes. As deformation trends of the investigated processes are extremely slow or very slow [43], a state of activity definition based only on geomorphological features is often not easy. However, slow displacements typical of post-failure residual deformation are most likely best observed by A-DInSAR [66], which allow observing and quantitatively measuring past displacements using archived SAR data. The application of the state of activity matrix (Figure 6) based on both ascending and descending contemporary datasets allowed for a better definition of the state of activity during the investigated periods (Figure 7), i.e., 1992–2010.

The state of activity matrix provided more objective information about the landslide state of activity than those showed in Figure 3b. A higher number of landslides were revealed as "active" by A-DInSAR results (Figure 7) than information attained using geomorphological data (Figure 4). The state of activity derived using traditional mapping techniques represents an information of a given condition limited at a well-defined moment (i.e., when the field survey takes place, or when the aerial photos are taken), while, the A-DInSAR investigation allows the observation of several processes over a much longer time interval. Moreover, it is possible to assess the state of activity condition starting from quantitative data related to the process itself (i.e., displacements measured with millimeter accuracy), not linked with observable, subjective effects on the ground. It is worth remembering that the activity matrix presented here is based on double and independent dataset results for each period (ascending and descending orbital geometries), thus allowing a more reliable outcome. Furthermore, it is worth noticing that the topographical effects related to steepness and slope orientation (able to cause radar distortions on the images used) are not very strong in the present case study. However, the results are insufficient for analyzing all of the landslide processes. In the present study, the lack of PSs in some areas is primarily linked to the local absence of targets characterized by good radar scattering behavior. In a strongly vegetated area, such as this one, it is evident that the presence of good scatters affects the A-DInSAR results more than any other radar or geomorphological parameter. As stated by Hanssen [75], A-DInSAR is an "opportunistic" technique; thus, when such a methodology is used to study non-urban areas (which is a very common and likely scenario for areas affected by landslide processes), the role played by potential good scatterers is fundamental. Moreover, it is very important to have available enough good targets in the area in order to also achieve a sufficient number of homogeneously distributed PSs over the landslide bodies under investigation. An example of detection without PSs is visible in the D ellipse in Figure 5, where no PSs are detected because no good scatterers are present. Consequently, several landslides that were recognized as active by the interpretation of multi-temporal aerial photos and geomorphologic field surveys have unfortunately not had their past displacements investigated by A-DInSAR data.

Finally, we want to stress that a deeper investigation on SAR images is sometimes required to analyze and better interpret the interferometric results, and sometimes this may be attained only by manually exploring time series of every measurement point and, when necessary, processing them with specific parameters.

6. Conclusions

Detailed remote sensing analyses, together with geomorphological field surveys, have been performed to extensively characterize landslide processes severely affecting a portion of the Dendalo stream basin approximately 20 km^2 large. The interpretation of multi-temporal aerial photos allowed the definition of the spatial and temporal evolution of the instability processes over the last five decades. Analyses of geomorphological features represented the first step towards attaining a basic knowledge of the number, typology, extension and mapping of these phenomena. Then, A-DInSAR analyses based on a mixed PSI/QPSI technique allowed substantially improving the information useful for landslide mapping. The SAR data from the ESA archive have been analyzed to extract information related to past displacements. We analyzed almost 220 SAR images divided into four datasets covering approximately 18 years of deformational history of the investigated area. Every SAR dataset was subject to an independent A-DInSAR processing; hence, the congruency of A-DInSAR results over same areas can be considered more robust and reliable.

More than 27 landslides covering a large portion of the basin have been successfully investigated using A-DInSAR. Using the ascending and descending datasets for the ERS (1992–2001) and Envisat (2003–2010) periods enabled the observation of the deformational processes affecting both the East and West facing slopes. A landslide activity matrix based on A-DInSAR results has been adopted to assess the past activity of the investigated landslides and then compared with the state of activity assessment made by standard geomorphological analyses. Moreover, by the combination of Ascending and Descending orbital geometries, the definition of the landslide kinematics characterized by the presence

of sufficient scatterers was possible. Finally, it is worth noticing that the combination of different observation geometries avoided the misleading interpretation of some processes characterized by ambiguous geomorphological features.

Based on what above, we can state that the investigated basin is characterized by more than 90 slope deformation phenomena. However, it is worth noting that according to our results the most vulnerable areas, mainly represented by urban settlements, located on the hilltops, can be considered not affected by deformation during the analyzed periods. In the underlying slopes, mainly facing E-W, different types of slope movements (earth-flows, slides and complex landslides) characterized by single or coalescent bodies and have been recorded. The related state of activity has been distinguished in active, inactive and undefined; among the active ones, detected velocity is up to 20 mm/year. The more active slope process is classified as roto-translational slide. It shows a sliding surface some tens of meters deep and a continuous horizontal deformation component in the lower part of the slope cumulating more than 30 cm in 18 years in the most active portion.

The methodological approach, successfully tested in the study area, can effectively extended to many other worldwide areas characterized by similar geological and geomorphological setting: outcropping of fine-grained jointed formations arranged in gentle slopes continuously cut by a dense hydrographic network and affected by slow movement such as slides, earth-flows and complex landslides.

To conclude, the A-DInSAR analyses and in particular PSI has proved to be effective for mapping and analyzing the landslide deformation patterns. Nowadays, PSI technique will experience a major development thanks to the Sentinel-1 (ESA) high-quality data, which will increase considerably the deformation monitoring potential. The large spatial coverage (swath of 250 km) is indeed very useful for study wide-areas, and thanks to the shorter temporal revisit time (six days, thanks to the double platform Sentinel 1A and 1B), Sentinel-1 data allow an improvement of the coherence, reducing the temporal decorrelation.

Author Contributions: Francesca Bozzano and Paolo Mazzanti supervised and coordinated the research and contributed to the article organization; Daniele Perissin and Alfredo Rocca designed and performed the A-DInSAR analyses; Pierfederico De Pari and Marco E. Discenza drafted the geological map and performed the landslide mapping. Alfredo Rocca and Paolo Mazzanti drafted the manuscript, which was revised by all authors.

Conflicts of Interest: The authors declare no conflicts of interest.

References

1. Fiorucci, F.; Cardinali, M.; Carlà, R.; Rossi, M.; Mondini, A.C.; Santurri, L.; Ardizzone, F.; Guzzetti, F. Seasonal landslide mapping and estimation of landslide mobilization rates using aerial and satellite images. *Geomorphology* **2011**, *129*, 59–70. [CrossRef]

2. Guzzetti, F.; Mondini, A.C.; Cardinali, M.; Fiorucci, F.; Santangelo, M.; Chang, K.T. Landslide inventory maps: New tools for an old problem. *Earth Sci. Rev.* **2012**, *112*, 42–66. [CrossRef]

3. Jaboyedoff, M.; Oppikofer, T.; Abellán, A.; Derron, M.H.; Loye, A.; Metzger, R.; Pedrazzini, A. Use of LIDAR in landslide investigations: A review. *Nat. Hazards* **2012**, *61*, 5–28. [CrossRef]

4. Cigna, F.; Bianchini, S.; Casagli, N. How to assess landslide activity and intensity with Persistent Scatterer Interferometry (PSI): The PSI-based matrix approach. *Landslides* **2012**, *10*, 267–283. [CrossRef]

5. Varnes, D.J. *The Logic of Geological Maps, with Special Reference to their Interpretation and Use for Engineering Purposes*; U.S. Geological Survey Professional Paper; United States Government Printing Office: Washington, WA, USA, 1974; p. 48.

6. Varnes, D.J. *Landslide Hazard Zonation: A Review of Principles and Practice*; Unesco: Paris, France, 1984; pp. 1–63.

7. Rockaway, J.D. The influence of map scale on engineering geologic mapping. *Bull. Int. Assoc. Eng. Geol.* **1976**, *13*, 119–122. [CrossRef]

8. Parise, M. Landslide mapping techniques and their use in the assessment of the landslide hazard. *Phys. Chem. Earth Part C* **2001**, *26*, 697–703. [CrossRef]

9. Singh, L.P.; Van Westen, C.J.; Ray, P.C.; Pasquali, P. Accuracy assessment of InSAR derived input maps for landslide susceptibility analysis: A case study from the Swiss Alps. *Landslides* **2005**, *2*, 221–228. [CrossRef]

10. Kampes, B.M. *Radar Interferometry Persistent Scatterers Technique*; Springer: Dordrecht, The Netherlands, 2006.

11. Lauknes, T.; Shanker, A.P. Detailed rockslide mapping in northern Norway with small baseline and persistent scatterer interferometric SAR time series methods. *Remote Sens. Environ.* **2010**, *114*, 2097–2109. [CrossRef]

12. Cigna, F.; Del Ventisette, C.; Liguori, V.; Casagli, N. Advanced radar-interpretation of InSAR time series for mapping and characterization of geological processes. *Nat. Hazards Earth Sys. Sci.* **2011**, 865–881. [CrossRef]

13. Bozzano, F.; Rocca, A. Remote monitoring of deformation using Satellite SAR Interferometry. *Geotech. News* **2012**, *30*, 26.

14. Rocca, A.; Mazzanti, P.; Perissin, D.; Bozzano, F. Detection of past slope activity in a desert area using multi-temporal DInSAR with ALOS PALSAR data. *Ital. J. Eng. Geol. Environ.* **2014**, *1*, 35–50. [CrossRef]

15. Ferretti, A.; Prati, C.; Rocca, F. Permanent scatterers in SAR interferometry. *IEEE Trans. Geosci. Remote Sens.* **2001**, *39*, 8–20. [CrossRef]

16. Berardino, P.; Fornaro, G.; Lanari, R.; Sansosti, E. A new algorithm for surface deformation monitoring based on small baseline differential SAR interferograms. *IEEE Trans. Geosci. Remote Sens.* **2002**, *40*, 2375–2383. [CrossRef]

17. Perissin, D.; Wang, T. Repeat-Pass SAR Interferometry with Partially Coherent Targets. *IEEE Trans. Geosci. Remote Sens.* **2012**, *50*, 271–280. [CrossRef]

18. Del Ventisette, C.; Righini, G.; Moretti, S.; Casagli, N. Multitemporal landslides inventory map updating using spaceborne SAR analysis. *Int. J. Appl. Earth Obs. Geoinf.* **2014**, *30*, 238–246. [CrossRef]

19. Farina, P.; Casagli, N.; Ferretti, A. Radar-interpretation of InSAR measurements for landslide investigations in civil protection practices. In Proceedings of the First North American Landslide Conference, Vail, CO, USA, 3–8 June 2007; pp. 272–283.

20. Notti, D.; Davalillo, J.C.; Herrera, G.; Mora, O. Assessment of the performance of X-band satellite radar data for landslide mapping and monitoring: Upper Tena Valley case study. *Nat. Hazards Earth Syst. Sci.* **2010**, *10*, 1865–1875. [CrossRef]

21. Mazzanti, P.; Rocca, A.; Bozzano, F.; Cossu, R.; Floris, M. Landslides forecasting analysis by time series displacement derived from satellite InSAR data: Preliminary results. In Proceedings of the Fringe 2011 Workshop, Rome, Italy, 19–23 September 2011.

22. Strozzi, T.; Ambrosi, C.; Raetzo, H. Interpretation of aerial photographs and satellite SAR interferometry for the inventory of landslides. *Remote Sens.* **2013**, *5*, 2554–2570. [CrossRef]

23. Akbarimehr, M.; Motagh, M.; Haghshenas-Haghighi, M. Slope stability assessment of the sarcheshmeh landslide, Northeast Iran, investigated using inSAR and GPS observations. *Remote Sens.* **2013**, *5*, 3681–3700. [CrossRef]

24. Bigi, S.; Centamore, E.; Nisio, S. Elementi di tettonica quaternaria nell'area pedeappenninica marchigiano-abruzzese. *Il Quat.* **1997**, *10*, 359–362.

25. Di Bucci, D.; Tozzi, M. La linea "Ortona-Roccamonfina": Revisione dei dati esistenti e nuovi contributi per il settore settentrionale (Media valle del Sangro). *Studi Geol. Camerti* **1991**, *2*, 397–406.

26. Mostardini, F.; Merlini, S. Appennino centro-meridionale. Sezioni geologiche e proposta di un modello strutturale. *Mem. Soc. Geol. Ital.* **1992**, *35*, 177–202.

27. Patacca, E.; Scandone, P. Geology of the Southern Apennines. *Boll. Soc. Geol. Ital.* **2007**, *7*, 75–199.

28. Miccadei, E. Geologia dell'area Alto Sagittario-Alto Sangro. *Geol. Romana* **1993**, *29*, 463–481.

29. Scisciani, V.; Calamita, F.; Tavarnelli, E.; Rusciardelli, G.; Ori, G.G.; Paltrinieri, W. Foreland-dipping normal faults in the inner edges of syn-orogenic basins: A case from the Central Apennines, Italy. *Tectonophysics* **2001**, *330*, 211–224. [CrossRef]

30. Calamita, F.; Scisciani, V.; Montefalcone, R.; Paltrinieri, W.; Pizzi, A. L'ereditarietà, del paleomargine dell'Adria nella geometria del sistema orogenico centro-appenninico: L'area abruzzese esterna. *Mem. Soc. Geol. Ital.* **2002**, *57*, 355–368.

31. Demangeot, J. Géomorphologie des Abruzzes Adriatiques. In *Centre Recherche et Documentation Cartographique, Memoires et Documents*; CNRS: Paris, France, 1965; p. 403.

32. Fanucci, F.; Moretti, E.; Nesci, O.; Savelli, D.; Veneri, F. Tipologia dei terrazzi vallivi ed evoluzione del rilievo nel versante Adriatico dell'Appennino centro-settentrionale. *Il Quat.* **1996**, *9*, 255–258.

33. Farabollini, P.; Nisio, S. Evoluzione geomorfologica quaternaria del bacino del F. Vomano (Abruzzo). *Il Quat.* **1997**, *10*, 101–104.

34. Currado, C.; Fredi, P. Morphometric parameters of drainage basins and morphotectonic setting of eastern Abruzzo. *Mem. Soc. Geol. Ital.* **2000**, *55*, 411–419.

35. Centamore, E.; Nisio, S.; Prestininzi, A.; Scarascia Mugnozza, G. Evoluzione morfodinamica e fenomeni franosi nel settore periadriatico dell'Abruzzo settentrionale. *Studi Geol. Camerti* **1997**, *14*, 9–27.

36. Bigi, S.; Calamita, F.; Cello, G.; Centamore, E.; Deiana, G.; Paltrinieri, W.; Ridolfi, M. Evoluzione messinianopliocenica del sistema catena avanfossa dell'area marchigiano-abruzzese esterna. *Studi Geol. Camerti* **1995**, *1*, 29–35.

37. D'Alessandro, L.; Pantaleone, A. Caratteristiche geomorfologiche e dissesti nell'Abruzzo sud-orientale. *Mem. Soc. Geol. Ital.* **1987**, *37*, 805–821.

38. Buccolini, M.; Crescenti, U.; Sciarra, N. Interazione fra dinamica dei versanti ed ambenti costruiti: alcuni esempi in Abruzzo. *Il Quat.* **1994**, *7*, 179–196.

39. D'Alessandro, L.; Miccadei, E.; Piacentini, T. Morphostructural elements of central-eastern Abruzzi: contributions to the study of the role of tectonics on the morphogenesis of the Appennine chain. *Quat. Int.* **2003**, *101–102*, 115–124. [CrossRef]

40. Varnes, D.J. Slope Movement Types and Processes. In *Landslides, Analysis and Control. Special Report*; Schuster, R.L., Krizek, R.J., Eds.; Transportation and Road Research Board, Natural Academy of Sciences: Washington, DC, USA, 1978; pp. 11–33.

41. Autorità dei Bacini di Rilievo Regionale Dell'abruzzo e del Bacino Interregionale del Fiume Sangro. Piano Stralcio di Bacino Per L'assetto Idrogeologico dei Bacini Idrografici di Rilievo regionale Abruzzesi e del Bacino Interregionale del Fiume Sangro "Fenomeni Gravitativi e Processi Erosivi". Available online: http://autoritabacini.regione.abruzzo.it/index.php/pai (accessed on 20 December 2016).

42. ISPRA-Istituto Superiore per la Protezione e Ricerca Ambientale (2007). Progetto IFFI-Inventario dei Fenomeni Franosi in Italia. Available online: http://www.apat.gov.it/site/it-IT/Progetti/IFFI_-Inventario_dei_fenomeni_franosi_in_Italia/ (accessed on 20 December 2016).

43. Cruden, D.M.; Varnes, D.J. Landslide types and processes. *Landslides Investig. Mitig.* **1996**, *247*, 36–75.

44. Wieczorek, G.F. Preparing a detailed landslide-inventory map for hazard evaluation and reduction. *IAEG Bull.* **1984**, *21*, 337–342. [CrossRef]

45. Canuti, P.; Focardi, P. Slope stability and landslides investigation in Tuscany. *Mem. Soc. Geol. Ital.* **1986**, *31*, 307–315.

46. González-Díez, A.; Remondo, J.; de Teran, J.R.D.; Cendrero, A. A methodological approach for the analysis of the temporal occurrence and triggering factors of landslides. *Geomorphology* **1999**, *30*, 95–113. [CrossRef]

47. Guzzetti, F.; Carrara, A.; Cardinali, M.; Reichenbach, P. Landslide hazard evaluation: A review of current techniques and their application in a multi-scale study, Central Italy. *Geomorphology* **1999**, *31*, 181–216. [CrossRef]

48. Parise, M.; Wasowski, J. Landslide activity maps for landslide hazard evaluation: Three case studies from Southern Italy. *Nat. Hazards* **1999**, *20*, 159–183. [CrossRef]

49. Massonnet, D.; Rossi, M.; Carmona, C.; Adragna, F.; Peltzer, G.; Feigl, K.; Rabaute, T. The displacement field of the Landers earthquake mapped by radar interferometry. *Nature* **1993**, *364*, 138–142. [CrossRef]

50. Massonnet, D.; Feigl, K.; Rossi, M.; Adragna, F. Radar interferometric mapping of deformation in the year after the Landers earthquake. *Nature* **1994**, *369*, 227–230. [CrossRef]

51. Massonnet, D.; Briole, P.; Arnaud, A. Deflation of Mount Etna monitored by spaceborne radar interferometry. *Nature* **1995**, *375*, 567–570. [CrossRef]

52. Antonielli, B.; Monserrat, O.; Bonini, M.; Righini, G.; Sani, F.; Luzi, G.; Feyzullayev, A.A.; Aliyev, A.S. Pre-eruptive ground deformation of Azerbaijan mud volcanoes detected through satellite radar interferometry (DInSAR). *Tectonophysics* **2014**, *637*, 163–177. [CrossRef]

53. Goldstein, R.; Engelhardt, H.; Kamb, B.; Frolich, R. Satellite radar interferometry for monitoring ice-sheet motion: application to an Antarctic ice stream. *Science* **1993**, *262*, 1525–1530. [CrossRef] [PubMed]

54. Kwok, R.; Fahnestock, M.A. Ice sheet motion and topography from radar interferometry. *IEEE Trans. Geosci. Remote Sens.* **1996**, *34*, 189–200. [CrossRef]

55. Strozzi, T.; Farina, P.; Corsini, A.; Ambrosi, C.; Thüring, M.; Zilger, J.; Wiesmann, A.; Wegmuller, U.; Werner, C. Survey and monitoring of landslide displacements by means of L-band satellite SAR interferometry. *Landslides* **2005**, *2*, 193–201. [CrossRef]

56. Strozzi, T.; Delaloye, R.; Kääb, A.; Ambrosi, C.; Perruchoud, E.; Wegmüller, U. Combined observations of rock mass movements using satellite SAR interferometry, differential GPS, airborne digital photogrammetry, and airborne photography interpretation. *J. Geophys. Res. Earth Surf.* **2010**, *115*. [CrossRef]

57. García-Davalillo, J.C.; Herrera, G.; Notti, D.; Strozzi, T.; Álvarez-Fernández, I. DInSAR analysis of ALOS PALSAR images for the assessment of very slow landslides: The Tena Valley case study. *Landslides* **2014**, *11*, 225–246. [CrossRef]

58. Jebur, M.N.; Pradhan, B.; Tehrany, M.S. Using ALOS PALSAR derived high-resolution DInSAR to detect slow-moving landslides in tropical forest: Cameron Highlands, Malaysia. *Geomat. Nat. Hazards Risk* **2013**, 741–759. [CrossRef]

59. Ferretti, A.; Fumagalli, A.; Novali, F.; Prati, C.; Rocca, F.; Rucci, A. A new algorithm for processing interferometric data-stacks: SqueeSAR. *IEEE Trans. Geosci. Remote Sens.* **2011**, *49*, 3460–3470. [CrossRef]

60. Hooper, A.; Zebker, H.; Segall, P.; Kampes, B. A new method for measuring deformation on volcanoes and other natural terrains using InSAR persistent scatterers. *Geophys. Res. Lett.* **2004**, *31*, L23611. [CrossRef]

61. Lauknes, T.R. Long-Term Surface Deformation Mapping Using Small-Baseline Differential SAR Interferograms. Master's Thesis, University of Tromso, Tromsø, Norway, 2004. Unpublished work.

62. Van Leijen, F.J.; Hanssen, R.F. Persistent scatterer density improvement using adaptive deformation models. In Proceedings of IEEE International Geoscience and Remote Sensing Symposium, Barcelona, Spain, 23–27 July 2007; pp. 2102–2105.

63. Perissin, D. Validation of the submetric accuracy of vertical positioning of PSs in C-band. *IEEE Geosci. Remote Sens. Lett.* **2008**, *5*, 502–506. [CrossRef]

64. Perissin, D.; Wang, Z.; Wang, T. The SARPROZ InSAR tool for urban subsidence/manmade structure stability monitoring in China. In Proceedings of the ISRSE 2010, Sidney, Australia, 10–15 April 2011.

65. Ferretti, A.; Prati, C.; Rocca, F.; Nicola, C.; Farina, P.; Young, B. Permanent Scatterers technology: a powerful state of the art tool for historic and future monitoring of landslides and other terrain instability phenomena. In Proceedings of the International Conference on Landslide Risk Management, Vancouver, BC, Canada, 31 May–2 June 2005; AA Balkema: Vancouver, BC, Canada.

66. Colesanti, C.; Wasowski, J. Investigating landslides with space-borne Synthetic Aperture Radar (SAR) interferometry. *Eng. Geol.* **2006**, *88*, 173–199. [CrossRef]

67. Cascini, L.; Fornaro, G.; Peduto, D. Advanced low- and full-resolution DInSAR map generation for slow-moving landslide analysis at different scales. *Eng. Geol.* **2010**, *112*, 29–42. [CrossRef]

68. Farina, P.; Colombo, D.; Fumagalli, A.; Marks, F.; Moretti, S. Permanent Scatterers for landslide investigations: Outcomes from the ESA-SLAM project. *Eng. Geol.* **2006**, *88*, 200–217. [CrossRef]

69. Meisina, C.; Zucca, F.; Fossati, D.; Ceriani, M.; Allievi, J. Ground deformation monitoring by using the Permanent Scatterers Technique: The example of the Oltrepo Pavese (Lombardia, Italy). *Eng. Geol.* **2006**, *88*, 240–259. [CrossRef]

70. Righini, G.; Pancioli, V.; Casagli, N. Updating landslide inventory maps using Persistent Scatterer Interferometry (PSI). *Int. J. Remote Sens.* **2012**, *33*, 2068–2096. [CrossRef]

71. Bianchini, S.; Cigna, F.; Righini, G.; Proietti, C.; Casagli, N. Landslide hotspot mapping by means of persistent scatterer interferometry. *Environ. Earth Sci.* **2012**, *67*, 1155–1172. [CrossRef]

72. Tofani, V.; Raspini, F.; Catani, F.; Casagli, N. Persistent Scatterer Interferometry (PSI) Technique for Landslide Characterization and Monitoring. *Remote Sens.* **2013**, 1045–1065. [CrossRef]

73. Colombo, A.; Mallen, L.; Pispico, R.; Giannico, C.; Bianchi, M.; Savio, G. Mappatura regionale delle aree monitorabili mediante l'uso della tecnica PS. In Proceedings of the 10th National Conference ASITA, Bolzano, Italy, 14–17 November 2006.

74. Wasowski, J.; Bovenga, F. Investigating landslides and unstable slopes with satellite Multi Temporal Interferometry: Current issues and future perspectives, *Eng. Geol.* **2014**, *174*, 103–138. [CrossRef]

75. Hanssen, R.F. Satellite radar interferometry for deformation monitoring: a priori assessment of feasibility and accuracy. *Int. J. Appl. Earth Obs. Geoinf.* **2005**, *6*, 253–260. [CrossRef]